International Journal of Heat and Mass Transfer 52 (2009) 4929–4937

Contents lists available at ScienceDirect

International Journal of Heat and Mass Transfer

journal homepage: www.elsevier.com/locate/ijhmt

Gaseous bubble nucleation under shear flow

Ho-Young Kwak *, Ki-Moon Kang

Mechanical Engineering Department, Chung-Ang University, Seoul 156-756, Republic of Korea

ARTICLE INFO

Article history:
Received 24 December 2008
Received in revised form 28 April 2009
Available online 4 July 2009

Keywords:
Decompression experiment
Degassing
Gaseous bubble nucleation
Shear flow
Surfactant
Supersaturated solution

ABSTRACT

A decompression experiment of a water solution, saturated with methane gas at about 68 atm at room temperature, was done to investigate gas bubble nucleation under shear flow. A pressure reduction from 68 atm to atmospheric pressure is well below the decompression pressure required for spontaneous bubble nucleation of the methane gas, about 120 atm. The application of a shear flow from 5 min before to 1 min after the decompression induced active bubble formation and the final gas content in the solution was reduced substantially, even with the application of low shear rate of 25/s. However, the addition of the surfactant to the solution, which reduces interfacial tension considerably, hindered the bubble nucleation process.

1. Introduction

Understanding the degassing process from supersaturated liquid–gas solution is very important in many engineering applications. For example, industrial applications include degassing from molten metals [1] and the manufacture of foamed materials [2,3]. In the field of physiology, nitrogen bubble formation in blood vessels and tissue, as a result of an excessive rate of decompression, causes caisson disease [4]. Degassing from a supersaturated solution, the gaseous bubble is formed by an aggregation process involving the dissolved gas molecules, and is quite different from boiling or cavitation phenomena, a typical phase change process [5].

Systematic experiments on gas bubble formation from a highly supersaturated liquid–gas solution have been done by Hemmingsen [6,7]. He investigated bubble formation in a capillary tube (diameter of 0.15–2.5 mm) from a water–gas solution which was decompressed to atmospheric pressure from an initial saturated state at high pressure. After a series of such decompression experiments with different values for the initial saturation pressure, quite different threshold pressures for bubble nucleation were obtained for different dissolved gas species. These findings are quite contradictory to the predicted values from the classical nucleation theory. A condition of "massive bubble formation" was obtained when the initial saturation pressure was 20–30 atm higher than the threshold value. Also, it was observed that the capillary diameter affected the threshold value for bubble nucleation. For nitrogen, the threshold pressure dropped to 100 atm using a 2.5-mm diameter capillary tube, while the threshold value obtained was 170 atm for a 1.1-mm capillary. In these experiments, the pressure reduction time was reported as 2–3 s; however, the bubble formation time was not given.

Kaddah and Robertson [8] studied gas bubble nucleation in molten iron. In their experiment, a levitated molten iron drop was in equilibrium with dissolved gas at high pressure. By a sudden decrease in the pressure, the droplet becomes supersaturated. Nitrogen bubble nucleation in molten iron having an enormous high surface tension value was observed when the initial saturation pressure was about 53 atm, even though this result was not repeatable. On the other hand CO gas bubble nucleation in Fe–C–O melts was observed at an initial gas pressure as low as 10 atm, which cannot be explained by the classical theory of bubble nucleation with a macroscopic surface tension value [9].

The effect of shear on nucleation of bubbles, droplets, and of crystals has drawn some attention recently and is still a debated subject [10]. A theoretical study by Reguera and Rubi [11] revealed that shear flow may enhance the diffusivity of molecules and, correspondingly, the nucleation rate. Particularly, the shear promotes a drastic change in the crystallization process of polymers having high viscosity. However, the effect is expected to be unimportant in condensation. Indeed, a factor of 10 in nucleation of isoactic polypropylene was observed at a rate of shear 14/s compared with the stationary case [12]. Another computational study for a van der Waals fluid has revealed that shear affects the bubble growth rate due to enhanced molecular transport, but has little effect on the bubble nucleation process [13]. The nucleation and growth of a bubble in a Newtonian liquid having very high viscosity were

* Corresponding author. Fax: +82 2 826 7464.
E-mail address: kwakhy@cau.ac.kr (H.-Y. Kwak).

0017-9310/$ - see front matter © 2009 Elsevier Ltd. All rights reserved.
doi:10.1016/j.ijheatmasstransfer.2009.06.002

Nomenclature

A_n	surface area of n-mer cluster
F_n	free energy needed to form n-mer cluster
f_L	lost degree-of-freedom of a dissolved gas molecule in solution
H	Henry's constant
J_n	nucleation rate of n-mer cluster
k_B	Boltzmann constant
n	number of molecules in a n-mer cluster
n_b	number of molecules inside a bubble
n_c	number of molecules in a critical cluster
N_g	number density of dissolved molecules in solution
N_w	number density of water molecules in solution
P_i	initial saturation pressure
P_f	final saturation pressure
R_1	radius of aluminum rod
R_2	radius of test tube
r_g	radius of dissolved molecule
T	solution temperature
T_a	Taylor number
T_c	critical temperature of solution
t_{nu}	duration of nucleation process
V_g	molecular volume of a dissolved molecule
x_f	mole fraction of methane gas in water solution after nucleation process
x_i	mole fraction of methane gas saturated at 68 atm
x_o	mole fraction of methane gas in water solution saturated at atmospheric pressure
Greek letters β_g	accommodation coefficient
σ_g	surface tension of solution
σ_{LJ}	Lennard–Jones hard sphere diameter
v	dynamic viscosity of liquid
Ω_1	rotation speed of the aluminum rod

studied under simple shear and creeping flow using a Couette apparatus by Favelukis et al. [14]. They found that the growth rate of a slender bubble increases as the shear rate increases in the shear rate ranges between 2.0/s and 14.0/s.

In this study, decompression of a water solution saturated with methane gas at about 68 atm (1000 psi) at room temperature was done under shear flow. A shear stress by a Couette flow apparatus was imposed to investigate the shear effect on the bubble nucleation. This pressure reduction from 68 atm to atmospheric pressure is far below that required for spontaneous bubble formation for the methane gas, about 120 atm [5,15]. A shear flow was applied 5 min before to 1 min after the decompression and the final gas content in the solution was measured and it was found to be reduced substantially, even with application of a low shear rate of 25/s. For complete degassing, which is very hard usually, the decompression experiment at elevated temperature and accompanying with ultrasound irradiation was also performed.

2. Bubble nucleation theory

Classical nucleation theory was modified to produce a gaseous bubble formation model [5] and a vapor bubble formation model [15]. The essential element of these models is that the surface energy for formation of the critical cluster in the metastable state is formulated by molecular concepts, while the kinetic formalism of the classical theory is retained. However, a completely different physical mechanism is postulated for gas bubble formation in the gas–liquid solution and for vapor bubble formation in liquid [15]. For gas bubble formation in the supersaturated liquid–gas solution, the aggregation process of the dissolved gas molecules is the very first process for bubble formation.

Consider a liquid–gas solution saturated with gas at pressure P_i at temperature T. As a result of pressure reduction to P_f, the dissolved gases become supersaturated. In this metastable state, the dissolved gases aggregate into clusters. The driving force for this clustering process is just the chemical potential difference between the metastable state and the initial saturated state, which is given explicitly by

$$\mu_m - \mu_s = V_g(P_f - P_i) \tag{1}$$

Assuming that the chemical potential of the molecules in the clusters is the same as the chemical potential of the dissolved gas molecules in the metastable state, the free energy involved in the clustering process at the supersaturated condition due to the decompression process is given by [5]

$$F_n = -(P_i - P_f)nV_g + \frac{f_L}{2}k_BTn^{2/3} \tag{2}$$

The second term in the RHS of Eq. (2) represents the energy needed for the separation of the cluster from the solvent molecules. This energy is the part of translational motion energy constrained during the dissolution process [16]. A fact that the translational motion energy is the surface energy needed for one molecule cluster to overcome for bubble formation was shown by a heuristic approach [5]. Comparing the above equation to the capillary approximation, the molecular surface tension related to bubble nucleation of the dissolved molecules may be given as follows [17].

$$\sigma_g = \frac{r_g}{2}\left(\frac{f_L}{3}\frac{k_BT}{V_g}\right) \tag{3}$$

The "lost degree-of-freedom" f_L in Eq. (2) represents the degree of translational motion restrained in solution, given by [5,17]

$$\frac{f_L}{3} = \frac{\hat{V}_g}{V_g} \tag{4}$$

If a dissolved gas molecule occupies the equilibrium volume, $\hat{V}_g$ which is equal to $\pi(2^{1/6}\sigma_{LJ})^3/6$, all the three degree-of-freedom of translational motion is restrained. Somehow the molecule occupies more volume than the equilibrium volume, a part of the degree of translational motion will be restrained. The hard sphere diameter $(2^{1/6}\sigma_{LJ})$ for the volume that a single molecule occupies in solution is well defined quantity [18]. The condition for a maximum with respect to n in the free energy is found from Eq. (2) to be

$$(P_i - P_f)n_c^{1/3} = \frac{f_L}{3}\frac{k_BT}{V_g} \tag{5}$$

By substituting Eq. (5), the stability condition of the cluster, into Eq. (2), one may obtain the free energy needed to form the critical cluster such as

$$\frac{F_{n_c}}{k_BT} = \frac{f_L}{6}n_c^{2/3} \tag{6}$$

The growth of a cluster in the supersaturated solution depends on kinetic events within the liquid. Assuming that the mean velocity of the dissolved gas molecules and the number of activated gas

molecules per unit volume in solution depend on solution properties, one may get the steady state nucleation rate of the n_c-mer cluster by dissolved gases [19] with our surface energy as

$$J_{n_c} = Z_{fg} D_{fg} N_g \exp\left(-\frac{f_L}{6} n_c^{2/3}\right) \tag{7}$$

Here D_{fg} is rate that molecules strike the surface area of the cluster and Z_{fg} is the Zeldovich nonequilibrium factor [20]. D_{fg} in Eq. (7) is the rate molecules strike the surface area of the cluster, given by

$$D_{fg} = \frac{\beta_g}{4} \overline{V} \overline{N}_g A_n \tag{8}$$

In Eq. (8), $\overline{V}$ is the average speed of gas molecules within the solution, $\overline{N}_g$ is the number of activated gas molecules per unit volume and A_n is the n-mer cluster surface area given as $A_n = 4\pi r_n^2 = 4\pi r_g^2 n^{2/3}$. The accommodation coefficient β_g was taken to be unity. In fact, the pre-exponential factor in Eq. (7) is insensitive in determining the decompression amount for gaseous bubble formation.

The classical nucleation theory with macroscopic surface tension and the kinetic process by capturing or losing a molecule at the interface provides the following nucleation rate for the critical size bubble [9].

$$J_{r_c} = N_g \sqrt{\frac{\sigma}{2 m_g B}} \exp\left[-\frac{4\pi r_c^2 \sigma}{3 k_B T}\right] \tag{9}$$

where $B = 2/3$ and r_c in Eq. (9) is the radius of the critical size bubble, which is given by

$$r_c = \frac{2\sigma}{P_g - P_f} \tag{10}$$

The gas pressure inside the critical bubble may be obtained from the Kelvin equation such as [5,17]

$$P_g = P_i \exp\left[-\frac{V_g (P_i - P_f)}{k_B T}\right] \tag{11}$$

It should be noted that the decompression amount for the gaseous bubble formation with the classical nucleation theory given from Eqs. (9) and (10) by replacing P_g as P_i is about 1600 atm for any gas species dissolved in water having surface tension value of 0.072 N/m at room temperature.

A procedure to obtain the bubble nucleation rate from the molecular cluster model [5] is as follows. With an assumed value of the nucleation rate, J_{n_c}, one can calculate the number of molecules constituting the critical cluster, n_c from Eq. (7) and thereafter decompression amount, $P_i - P_f$, for bubble nucleation from Eq. (5) if the values of $\hat{V}_g$ and $V_g(T)$ are provided. The molecular volume $\hat{V}_g$ which restrains all the translational motion of a gas molecule in solution may be obtained from the hard sphere diameter of a molecule [5,17]. This molecular cluster model predicts pressure reduction required for bubble formation in various gas–water solutions, and that depends crucially on the occupied volume of the solute species in solution [6,7]. For example, a decompression amount of 360 atm is required for massive bubble formation in water for helium gas. On the other hand, it needs only 120 atm for methane gas. Furthermore, this model predicts the CO gas bubble formation in Fe–C–O melts [21] and bubble nucleation and subsequent formation of microcellular foam in polymer solutions [22]. More importantly, this model bridges the gap between the bubble embryo (a critical cluster) and the critical bubble [22,23], which was proposed in the classical theory. Once the transition from a cluster to a critical bubble takes place, subsequent growth to macroscopic size bubble can be done by diffusion process through the concentration defect at the bubble wall. A detailed exposition on the molecular cluster model can be found in Kwak [24].

3. Experimental apparatus and procedures

A schematic diagram of the test equipment for the decompression experiment is shown in Fig. 1. The test chamber is made of carbon steel. Two flat glass window 17.7 mm thick allow viewing of the sample during the decompression experiment. To receive the sample solution, a test tube was inserted into the test chamber from the bottom.

The saturated water–gas solution was prepared in a separate mixing cylinder (500 cc), made of stainless steel. The cylinder was filled with deionized water. A magnetic stirrer was used to mix the water and methane gas. Mixing was started by opening valve (5) slowly. The typical mixing time was 6 h. Next, the test chamber was purged and pressurized with methane gas by opening valve (2). After mixing was accomplished, the valve (2) is closed and the test section pressure was decreased slightly by

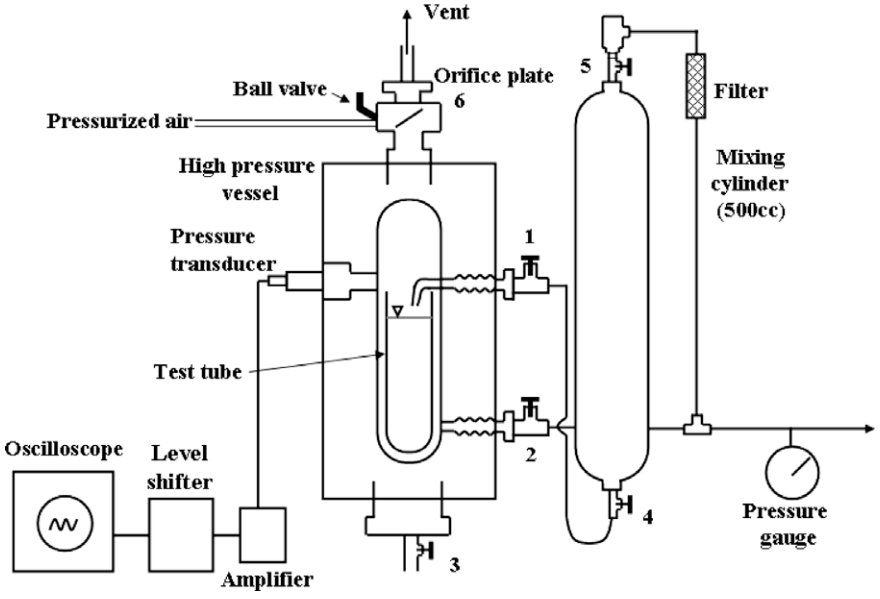

Fig. 1. Schematic diagram of decompression experiment.

opening valve (3). Then the mixture flows into the test tube by opening valve (1) and (4). About 6 cc of the water–methane gas solution was used in each experiment. After filling the test tube with the solution, valve (1) and (2) were closed to isolate the test chamber.

A Couette flow apparatus imposes a shear stress in a fluid without changing the pressure in the fluid, as shown in Fig. 2. The apparatus consists of an annulus formed by inserting a mirror finished aluminum rod with diameter of 7.94 mm into the center of the test tube. The shear flow is set up by rotating the rod by a small electric motor. The motor located at the top of the test chamber was attached to a gear box, and the speed was controlled by a variable DC voltage. The rotating rod was connected to a gear box with a 22:1 gear ratio. To eliminate the friction of the rotating rod, the end of the test tube was made of aluminum and fitted with a bearing.

The speed of the rotating rod was measured with a digital strobe, and found to be 240–1200 rpm. Speed below 240 rpm could not be operated. The corresponding shear rates are 20–100/s and Taylor numbers are 37,120–928,000. The rotating speed of the rod was found to be linearly dependent on the input voltage to the motor. It is known that a secondary flow called a Taylor vortex occurs if the rotation speed is above a critical value of the Taylor number, 33,000 in this case. The Taylor number for this particular case of rotating of inner cylinder only is defined as

$$T_a = \frac{4\Omega_1^2 R_1^4}{v^2(1-\eta^2)^2} \tag{12}$$

where $\eta = R_1/R_2$ and the radius of aluminum rod, R_1 is 3.97 mm and the radius of the test tube, R_2 is 6.75 mm. The Taylor vortices were observed at all rotation speeds tested and at a speed of 600 rpm, the wiggly pattern of the Taylor vortex was seen in an another test visualizing the flow pattern by using aluminum powder. This secondary flow is superimposed upon the main shear flow but is very weak in most instances. The time we imposed the shear flow field was 5 min before to 1 min after the decompression.

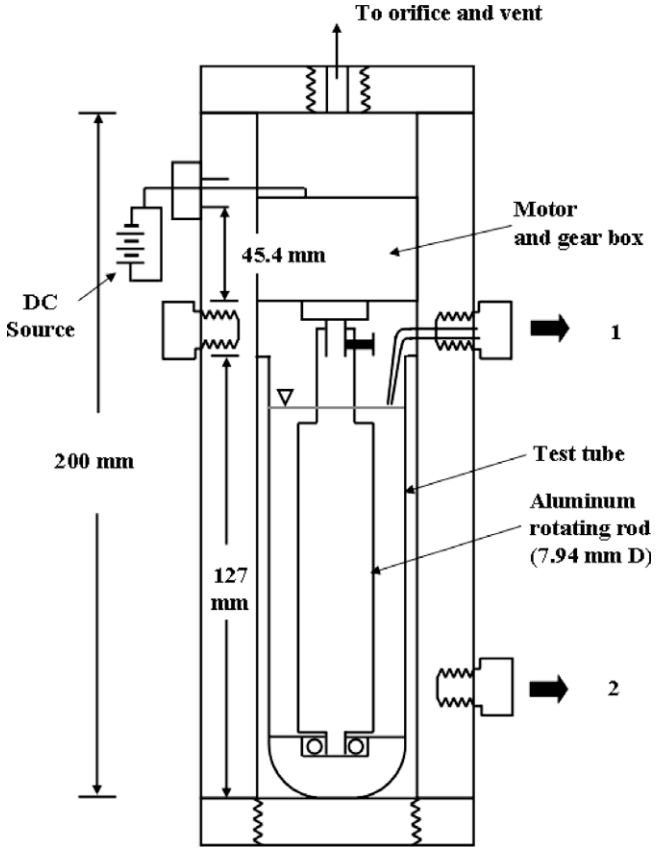

Fig. 2. Arrangement for shear flow experiments.

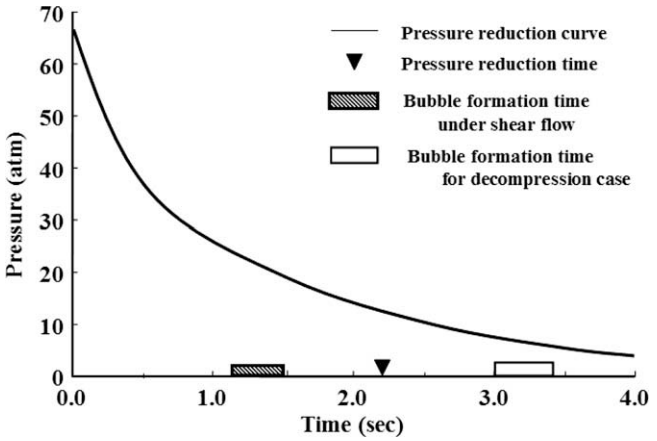

Fig. 3. Time dependent gas pressure inside the test chamber with an orifice diameter of 0.81-mm.

The decompression process was started by opening a ball valve (6) equipped with a fast-action, automatic, compressed air operator, located above the top of the test chamber. A high speed camera (Fairchild, Model HS 401) was started just before the decompression process. The film speed employed was about 200–400 frames/s. A timing light with 100 cycles per second was used to indicate the time at the edge of the film. The rate at which the pressure in the test section dropped was controlled by the size of the orifice on the outlet side of the ball valve. In this experiment an 0.81-mm diameter orifice was used. A piezoelectric pressure transducer installed at the wall of the test chamber measured the pressure reduction rate in the test section. A typical decompression rate in the test section is shown in Fig. 3.

After the decompression experiment finished, an attempt was made to measure the final concentration of the dissolved gas using gas chromatography (Beckman) with some external modifications. This modification consisted of some equipment to separate the water from the gas before it entered the diffusion column in the gas chromatography setup. Reliable results were usually achieved if the concentration was less than about 10 times the saturated concentration equilibrated at atmospheric pressure. The mole fraction of methane gas in water solution was estimated by Henry's law, $P = Hx$, where P is equilibrium pressure in atm unit. The value of Henry's constant for water–methane solution at 25 °C is about 4.13×10^4 atm [25].

4. Experimental results and discussion

4.1. Decompression experiment

As shown in Fig. 2, the pressure–time decay curve in the test chamber was of an exponential type from which an exponential time constant (t_e) can be obtained. The pressure reduction time (t_p) is defined as twice as the exponential time, or $t_p = 2t_e$. A bubble formation time (t_b) is defined as the time required to detecting a group of bubble in the solution after initiation of the decompression. Bubble nucleation in the supersaturated solution developed from the solution with the equilibrium pressure of 68 atm scarcely occurred by decompression only so that the final concentration of the dissolved gas was hardly measured. In this case the bubble formation time is about 2.97 s. As shown in Fig. 4a, a countable num-

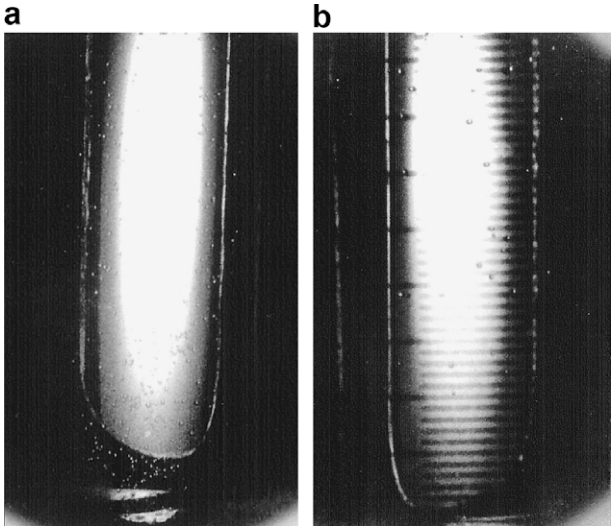

Fig. 4. Initial bubble formation stage for pure water at $t = 2.40$ s after decompression and for water mixed with a surfactant at $t = 3.60$ s after decompression. The bubble formation time in this case is $t_b = 1.83$ s.

Table 1
Shear flow experiments; initial saturation gas pressure is 68 atm where mole fraction of methane gas saturated with atmospheric pressure in water solution at 25 °C, x_o is 2.42×10^{-5}.

Test description	Rotation speed (RPM)	Bubble formation time, t_b (s)	$x_f \times 10^5$ final mole fraction	Level of concentration $\delta = x/x_o$	Remarks
Shear flow $t_p = 2.64$ s pure water	No rotation	2.97	50.4	20.8	Bubbles form on metal rotor surface only. One can hardly measure the residual concentration in this case
	300	1.46	12.6	5.21	Homogeneous bubble formation; bubbles can be seen inside tube
	600	1.30	7.8	3.22	
	900	1.19	7.2	2.98	
	1200	1.13	5.2	2.15	

ber of bubbles might be formed from the cavities on the surface of the test tube heterogeneously [26]. As is well known, gas cavities on the surface provide sites for bubble nucleation with lower energy barrier than that for homogeneous nucleation. In all these decompression tests, heterogeneous bubble formation occurred only a short period of time and the solution remained highly supersaturated.

4.2. Surfactant effect on gaseous bubble nucleation

In another series of tests, a surfactant (sodium-dodecyl-benzene-sulfonate) was added to the water–methane solution. For a very dilute surfactant concentration (1.5×10^{-4} g mol/l) a number of bubbles formed on the test tube surface as can be seen in Fig. 4b and the bubble growing process was inhibited. A further increase in the surfactant concentration hindered the nucleation process of the bubbles, and only 2–3 bubbles formed on the glass surface. With a surfactant concentration of 1.1×10^{-3} g mol/l which reduces the interfacial tension of water as much as 28 dyne/cm, no bubble formed even on the glass surface. This might be due to the fact that a surface active agent plays a role stabilizing the bubble nucleus [27]. The surfactant molecules surround the bubble nuclei to form a micelle and block the diffusion of the dissolved gas molecules to the bubble nuclei by which the nuclei grow. Similar result was observed for the CO bubble formation in iron melts: no bubble formation occurs provided that the surface of embryo is fully covered by surface active atoms [21]. This observed results indicate that aggregation of the dissolved gas molecules in the solution is the very first process for bubble formation [5,17]. This finding suggests that the classical theory with the macroscopic surface tension value [28] cannot explain the gaseous bubble nucleation events in solution. In fact, Briggs [29] observed that the tensile strength of water reduced very much near melting point where the surface tension becomes large.

4.3. Gaseous bubble nucleation under shear flow

The shear flow effect on bubble formation was found to be very effective. Bubble formation under the shear flow occurred earlier

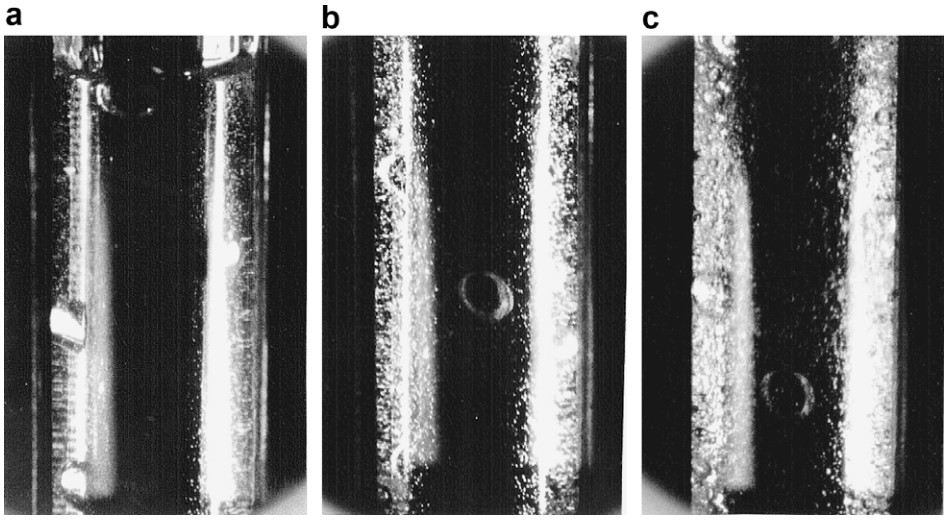

Fig. 5. Bubble nucleation and growing stage under shear flow at time (a) 2.16 s, (b) 3.16 s and (c) 4.66 s after decompression. In this case, the bubble formation time is $t_b = 1.46$ s.

than the decompression time, as shown in Fig. 3. Also the bubble formation time decreased as the rotation speed was increased as noted in Table 1. Active bubble formation always occurred and the final gas concentration in the solution reduced substantially even at the lowest speed of 300 rpm. A picture of the bubble formation at this speed is shown in Fig. 5. Many tiny bubbles move around the tube. A couple of large bubbles due to coalescence are also seen. The final supersaturation values decrease as the rotation speed increases from 300 to 1200 rpm, as confirmed in Table 1. The test results for the bubble formation in a shear flow field accompanying the decompression process are summarized in Table 1. The local heating due to the shearing action is certainly negligible for the speed ranges tested.

The decompression amount for massive bubble formation from a water–methane gas solution at 25 °C, calculated from Eqs. (4)–(6) with $J_{n_c} = 10^6/\text{cm}^3$, is about 120 atm [5]. This value is the exactly same as the observed value by Gerth and Hemmingsen [30]. The number of molecules inside a critical cluster is about 560 in this case. A molecular dynamics study yielded that the shearing action changed the liquid structure to stratify along the line of shear [31] so that the molecules are reordered to be staggered in the normal to the velocity gradient, as shown in Fig. 6. Such a structure rearrangement enhances the self-diffusion coefficient of the dissolved molecules and increases the dissolved gas volume occupied in the solution so that the decompression amount for bubble formation reduces correspondingly.

With a 20% increase in the effective diameter of the dissolved molecules, the decompression amount for massive bubble formation in the water–methane gas solution reduces to 70 atm from 120 atm, as verified in this experiment. In Table 2, given amount of decompression of 67 atm, the number of molecules constituting the critical cluster and the corresponding nucleation rate dependent on the applied shear rate are listed. A proper nucleation rate

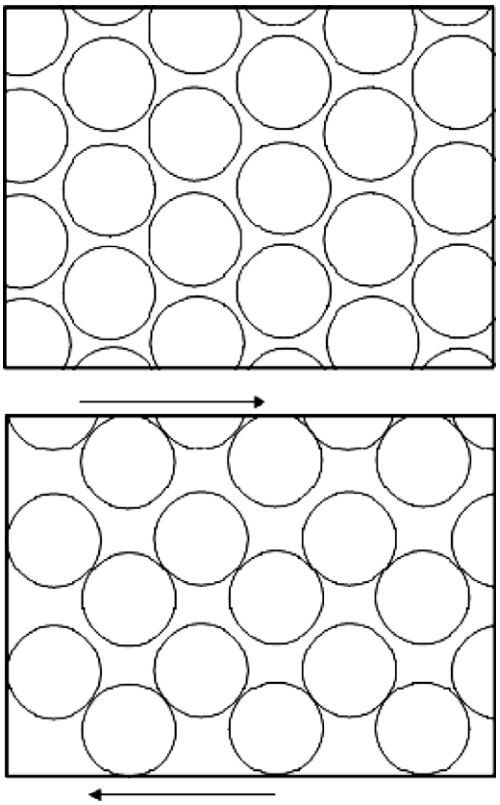

Fig. 6. A pictorial representation of the structural change of liquid molecules under shear flow by Heyes et al. (Ref. [31]).

Table 2
Possible fractions of volume changes and the corresponding number of molecules inside the critical clusters and their nucleation rates which are matched to the measured number of degassed methane molecules dependent on shear rates.

Shear rate (/s)	Fraction of volume change of dissolved molecule	Number of molecules inside the critical cluster, n_c	Nucleation rate of the critical cluster, J_{n_c}	Number of molecules degassed per unit volume calculated from Eq. (9)
25	0.21475	951.7	5.07×10^3	5.08×10^{19}
50	0.21490	951.0	5.19×10^3	5.24×10^{19}
75	0.21499	950.6	5.27×10^3	5.26×10^{19}
100	0.21505	950.3	5.31×10^3	5.29×10^{19}

J_{n_c} at given shear rate may be estimated from the measured number of degassed molecules per unit volume, which can be calculated by the RHS in the following equation.

$$J_{n_c} n_b t_{nu} = (x_i - x_f) N_w \tag{13}$$

where n_b is the number of molecules inside a 120-μm radius bubble which is developed from the critical cluster [22,23] and t_{nu} is nucleation duration of 60 s. With the estimated nucleation rate value, one may calculate the effective molecular volume of the dissolved gas in shear flow. As can be seen in Table 2, about 21.5% increase in the molecular volume of dissolved gas in shear flow. In the above equation x_i and x_f are the mole fractions of dissolved methane molecules at initial state saturated with 68 atm and at final state after the nucleation process, respectively. The bubble radius of 0.12 mm is just average bubble radius observed in the experiments. It is noted that narrow range of size distribution in bubble radius was observed in the bubble formation in polymer solution [23,32].

Even though the final mole fraction of methane gas is discernable depending on the amount of shear rate, the nucleation events are almost similar as confirmed in Table 2. This is because only a few percent difference in the number of degassed molecules exists between the low and high shear rates. Furthermore, the calculation results shown in Table 2 indicate that homogeneous nucleation might occur under shear flow because degassing of large amount of molecules from the solution cannot be possible through countable number of bubble formation on surface, or heterogeneous bubble nucleation. Certainly, the homogeneous bubble nucleation under shear flow cannot be explained by the classical nucleation theory because the interfacial tension remains constant under the flow.

4.4. Temperature dependence on bubble nucleation

As can be seen in Table 1, it is very hard to degassing the water-methane solution to the saturated condition at the ambient pressure. At high solution temperature up to 100 °C, the decompression experiment for the water–gas solution was done for possible complete degassing. Such high temperature of the test chamber was achieved by irradiation of power lamp. For steady state condition of the test chamber at a prescribed temperature was obtained after 3–5 h of irradiation.

One may calculate the temperature dependence of the decompression amount for bubble formation. Assume that the surface tension for the formation of the cluster, σ_g in Eq. (3), depends on the temperature according to an empirical power law [33] such as

$$\sigma_g = A\left(1 - \frac{T}{T_c}\right)^{\alpha} \tag{14}$$

where α is some power and A is some constant. With the above relation, the temperature dependence of the stability condition of the critical cluster becomes

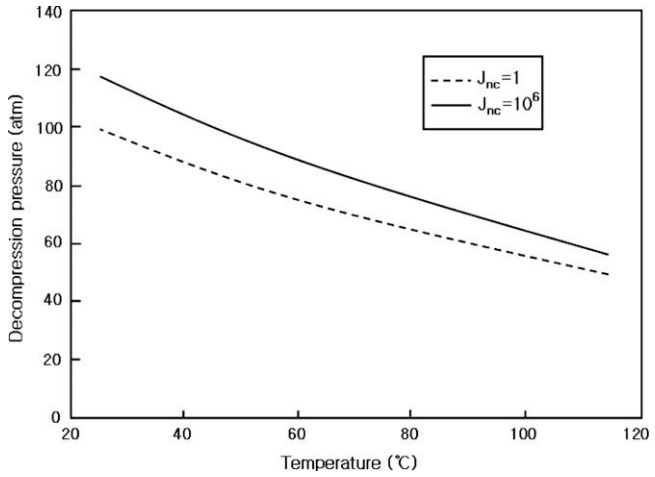

Fig. 7. Decompression pressure amount for bubble nucleation in water–methane solution depending solution temperature.

$$(P_i - P_f)n_c^{1/3} = \left(\frac{k_B T_{ref}}{V_{g,ref}}\right)\left(\frac{T_{ref}}{T}\right)\left(\frac{T_c - T}{T_c - T_{ref}}\right)^{6\alpha/5} \quad (15)$$

where $V_{g,ref}$ is the molecular volume of the dissolved molecule at a reference temperature T_{ref}, say 25 °C. With a value of $\alpha = 11/9$, the decompression amount with nucleation rate values of $J_{n_c} = 1$ and $J_{n_c} = 10^6$ are shown in Fig. 7. This figure indicates that massive bubble formation may occur around 80 °C with the decompression amount of 70 atm. Indeed, explosive bubble nucleation was observed at 80 °C at which vapor bubble nucleation hardly occurs as shown in Fig. 8. This observation shows vividly how the dissolved gas contents affect the bubble nucleation behavior in supersaturated solution at high temperature. However, such explosive bubble nucleation was not occurred at the solution temperature of 50 °C at which more heterogeneous nucleation occurred as shown in Fig. 9. In fact, previous study has revealed that the superheat limit of water 303 °C cannot be achieved experimentally due to the dissolved gases in solution [17]. The final concentration of the dissolved gases after decompression test at 80 °C is about $\delta = 2.55$.

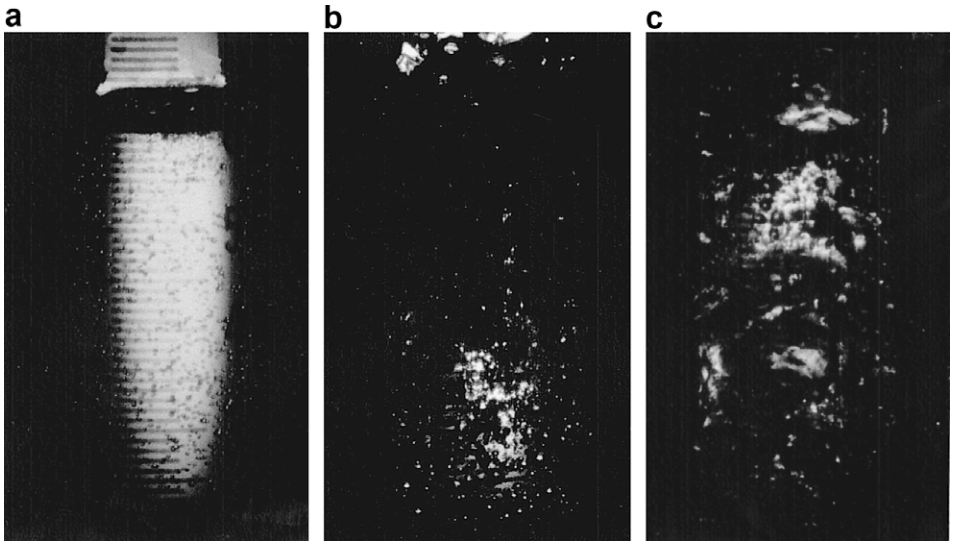

Fig. 8. Bubble nucleation and growing behavior in water–methane solution of temperature, 80 °C at time (a) 2.40 s, (b) 3.60 s and (c) 4.30 s after decompression from 68 atm. The bubble formation time in this case is $t_b = 1.83$ s.

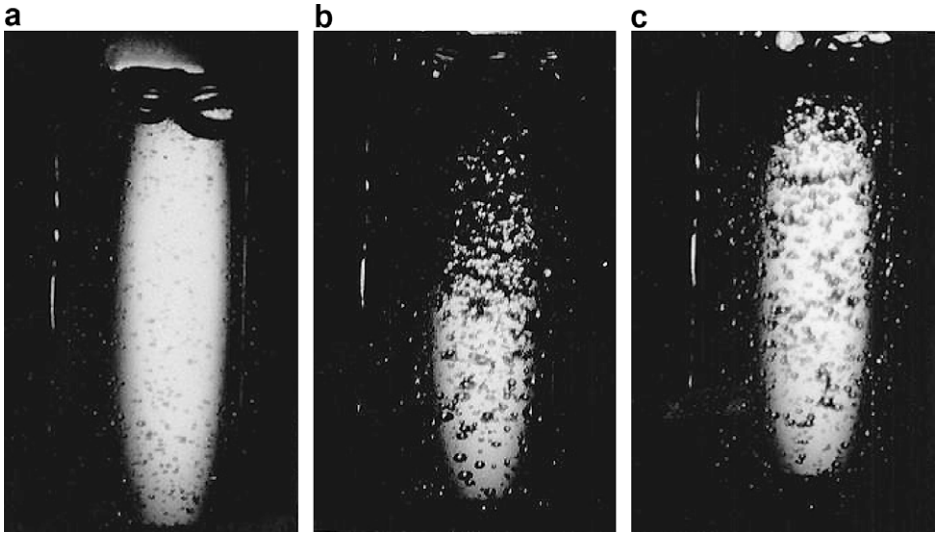

Fig. 9. Bubble nucleation and growing behavior in water–methane solution of temperature, 50 °C at time (a) 3.10 s, (b) 4.10 s and (c) 6.00 s after decompression from 68 atm. The bubble formation time is this case is $t_b = 2.44$ s.

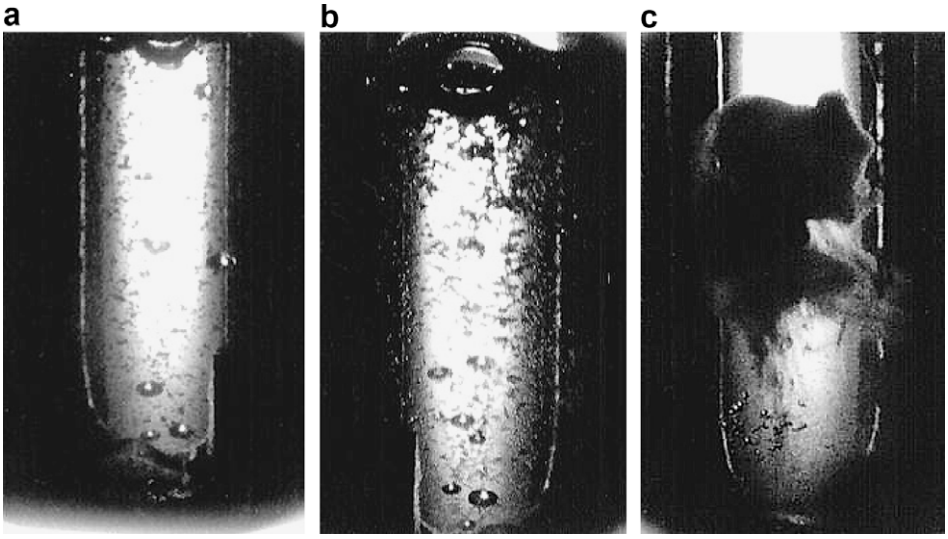

Fig. 10. Bubble nucleation process under ultrasonic field at time (a) 2.48 s, (b) 3.48 s with ultrasound frequency of 2.35 MHz and with 0.5 W power input and (c) 0.27 s ultrasound frequency of 1.65 MHz and with 4 W power input with 4 W input.

However, the level of the concentration saturated with atmospheric pressure ($\delta = 1.0$) was obtained for decompression test at 100 °C.

4.5. Decompression accompanying with ultrasonic fields

For complete degassing from the saturated water–methane solution at 68 atm, a decompression experiment accompanying with ultrasonic wave was also done. A disc type ultrasonic transducer (Channel Industries Inc., USA) was installed at the bottom of the test tube. Two different transducers with resonant frequencies of 2.35 MHz (0.89 mm thickness and 9.53 mm diameter) and 1.65 MHz (1.27 mm thickness and 9.53 mm diameter) were used. A function generator which was connected to a broadband power amplifier was used to operate the transducers.

When the ultrasonic power was relatively weak, below 0.5 W at 2.35 MHz, the bubble formation started slowly inside the solution as shown in Fig. 10a and b. The fine bubbles appeared in small irregularly shaped groups and the number of these groups gradually to darken the tube almost uniformly. At this low power input, the bubble formation time which was 1.26 s, was still well below the decompression time as shown in Fig. 3. The final mole fraction value of methane is about 2.43×10^{-4} in this case. Stronger ultrasonic power showed a strikingly different bubble formation behavior. A very short time after the decompression, a stream of fine bubbles was observed to flow from the bottom of the test tube. The bubble cloud expanded as it rose. Upon the reaching the top section of the test tube the cloud bend back and the upper part of the test tube would become dark with fine bubbles while a couple of cm of relatively clear liquid existed at the bottom. In most instances the entire test tube would eventually become dark with bubbles. Fig. 10c shows early stage of the bubble cloud. In this particular case of 4 W input power with 1.68 MHz frequency application after decompression, the level of concentration to the atmospheric pressure is about 0.94 or $\delta = 0.94$. Less explosive behavior of bubble formation was observed for the solution with addition of surfactant even though strong power of ultrasound was applied.

5. Conclusion

A decompression experiment of water–methane gas solution was done to investigate gas bubble formation under shear flow. The shearing action which changes the liquid structure stratifying along the line of shear promotes the bubble nucleation process quite a bit. It is understood that the dissolved gas molecules can occupy more volume in the shear layer where the interaction of solvent molecules is loosened. In another test, a concentration of 1.1×10^{-3} g mol/l of sodium-dodecyl-benzene-sulfonate, which can reduce the interfacial tension of water as much as 28 dynes/cm in the solution stopped the bubble nucleation process completely. This result indicates that aggregation of the dissolved molecules in the solution is the very first process for bubble nucleation of dissolved gases. For complete degassing below the saturation with the atmospheric pressure, high power ultrasound input to the solution is required.

Acknowledgement

This research was supported by the Chung-Ang University Research Grant in 2008.

References

[1] G.J. Kinsman, G.S.F. Hazeldean, M.W. Davies, Physicochemical factors affecting the vacuum deoxidation of steels, J. Iron Steel Inst. 207 (1969) 1463–1478.
[2] A.N. Gent, D.A. Tomkins, Nucleation and growth of gas bubbles in elastomers, J. Appl. Phys. 40 (1969) 2520–2525.
[3] J.S. Colton, N.P. Suh, The nucleation of microcellular thermoplastic foam with additives. Part I: Theoretical considerations, Polym. Eng. Sci. 27 (1987) 493–499.
[4] J.S. Haldane, J.G. Prisetly, Respiration, Yale University Press, New Haven, 1935.
[5] H. Kwak, R.L. Panton, Gas bubble nucleation in nonequilibrium in water–gas solutions, J. Chem. Phys. 78 (1983) 5795–5799.
[6] E.A. Hemmingsen, Cavitation in gas–supersaturated solutions, J. Appl. Phys. 46 (1975) 213–218.
[7] E.A. Hemmingsen, Spontaneous formation of bubbles in gas–supersaturated water, Nature 267 (1977) 141–142.
[8] N.H. El Kaddah, D.G.C. Robertson, Homogeneous nucleation of carbon monoxide bubbles in iron drops, J. Colloid Interface Sci. 60 (1977) 349–360.
[9] M. Blander, J.L. Katz, Bubble nucleation in liquids, AIChE J. 21 (1975) 833–848.
[10] R. Blaak, S. Auer, D. Frenkel, H. Lowen, Crystal nucleation of colloidal suspensions under shear, Phys. Rev. Lett. 93 (2004) 068303. 1–4.
[11] D. Reguera, J.M. Rubi, Homogeneous nucleation in inhomogeneous media. II: Nucleation in a shear flow, J. Chem. Phys. 119 (2003) 9888–9893.
[12] D. Yuya, T. Kikuchi, T. Inoue, Y. Iwai, A. Kawaguchi, Shear-enhanced nucleation of isoactic polypropylene in limited space, J. Macromol. Sci. Part B Phys. 45 (2006) 85–103.
[13] R.S. Qin, Bubble formation in lattice Boltzmann immiscible shear flow, J. Chem. Phys. 126 (2007) 114506. 1–5.
[14] M. Favelukis, Z. Tadmor, R. Semiat, Bubble growth in a viscous liquid in a simple shear flow, AIChE J. 45 (1999) 691–695.

[15] H. Kwak, R.L. Panton, Tensile strength of simple liquids predicted by a model of molecular interactions, J. Phys. D Appl. Phys. 18 (1985) 647–659.
[16] D.D. Eley, On the solubility of gases. Part I: The inert gases in water, Trans. Faraday Soc. 35 (1939) 1281–1293.
[17] H. Kwak, S. Oh, Gas–vapor bubble nucleation—a unified approach, J. Colloid Interface Sci. 278 (2004) 436–446.
[18] C. Owicki, H.A. Scheraga, Monte Carlo calculations in the isothermal–isobaric ensemble, 2. Dilute aqueous solution of methane, J. Am. Chem. Soc. 99 (1977) 7413–7418.
[19] J. Frenkel, Kinetic Theory of Liquids, Oxford University, London, 1946.
[20] J. Feder, K.C. Russel, J. Lothe, G.M. Pound, Homogeneous nucleation and growth of droplet in vapors, Adv. Phys. 15 (1966) 111–178.
[21] H. Kwak, S. Oh, A model of homogeneous bubble nucleation of CO bubbles in Fe–C–O melts, J. Colloid Interface Sci. 198 (1998) 113–118.
[22] K. Kim, S. Kang, H. Kwak, Bubble nucleation and growth in polymer solutions, Polym. Eng. Sci. 44 (2004) 1890–1899.
[23] H. Kwak, Y.W. Kim, Homogeneous nucleation and macroscopic growth of a gas bubble in organic solutions, Int. J. Heat Mass Transfer 41 (1998) 757–767.
[24] H. Kwak, Bubbles, Homogeneous Nucleation, in: P. Somasundaran (Ed.), Encyclopedia of Surface and Colloid Science, vol. 2, Taylor and Francis, Boca Raton, 2006, pp. 1048–1071.
[25] R.H. Perry, D.W. Green (Eds.), Perry's Chemical Engineers' Handbook, McGraw-Hill, New York, 1999.
[26] S.F. Jones, G.M. Evans, K.P. Galvin, Bubble nucleation from gas cavities—a review, Adv. Colloid Interface Sci. 80 (1999) 27–50.
[27] D.E. Yount, Skins of varying permeability: a stabilization mechanism for gas cavitation nuclei, J. Acoust. Soc. Am. 65 (1979) 1429–1439.
[28] S.D. Lubetkin, Why it is much easier to nucleate gas bubbles than theory predicted?, Langmuir 19 (2003) 2575–2587
[29] L.J. Briggs, Limiting negative pressure of water, J. Appl. Phys. 21 (1950) 721–722.
[30] W.A. Gerth, E.A. Hemmingsen, Gas supersaturation thresholds for spontaneous cavitation in water with gas equilibrium pressure up to 570 atm, Z. Narturforsch. 31a (1976) 1711–1716.
[31] D.M. Heyes, J.J. Kim, C.J. Montrose, T.A. Litovitz, Time dependent nonlinear shear stress effects in simple liquids: a molecular dynamics study, J. Chem. Phys. 73 (1980) 3987–3996.
[32] K. Kim, S. Kang, H. Kwak, Generation of microcellular foams by supercritical carbon dioxide in a PMMA compound, Int. Polym. Process. 23 (2008) 8–16.
[33] A.W. Adamson, Physical Chemistry of Surfaces, Interscience, New York, 1967.